ACS APPLIED MATERIALS & INTERFACES

Research Article

www.acsami.org

Nanostructured Electron-Selective Interlayer for Efficient Inverted Organic Solar Cells

Jiyun Song,[†,∥] Jaehoon Lim,[‡,§,∥] Donggu Lee,[†] M. Thambidurai,[†] Jun Young Kim,[†] Myeongjin Park,[†] Hyung-Jun Song,[†,§] Seonghoon Lee,[⊥] Kookheon Char,[*,‡] and Changhee Lee[*,†]

[†]Department of Electrical and Computer Engineering, Inter-university Semiconductor Research Center, Seoul National University, 1, Gwanak-ro, Gwanak-gu, Seoul 151-744, Korea

[‡]School of Chemical and Biological Engineering, The National Creative Research Initiative Center for Intelligent Hybrids, The WCU Program of Chemical Convergence for Energy & Environment, Seoul National University, 1, Gwanak-ro, Gwanak-gu, Seoul 151-744, Korea

[§]Chemistry Division, Los Alamos National Laboratory, Los Alamos, New Mexico 87545, United States

[⊥]School of Chemistry, Seoul National University, 1, Gwanak-ro, Gwanak-gu, Seoul 151-747, Korea

Supporting Information

ABSTRACT: We report a unique nanostructured electron-selective interlayer comprising of In-doped ZnO (ZnO:In) and vertically aligned CdSe tetrapods (TPs) for inverted polymer:-fullerene bulkheterojunction (BHJ) solar cells. With dimension-controlled CdSe TPs, the direct inorganic electron transport pathway is provided, resulting in the improvement of the short circuit current and fill factor of devices. We demonstrate that the enhancement is attributed to the roles of CdSe TPs that reduce the recombination losses between the active layer and buffer layer, improve the hole-blocking as well as electron-transporting properties, and simultaneously improve charge collection characteristics. As a result, the power conversion efficiency of PTB7:$PC_{70}BM$ based solar cell with nanostructured CdSe TPs increases to 7.55%. We expect this approach can be extended to a general platform for improving charge extraction in organic solar cells.

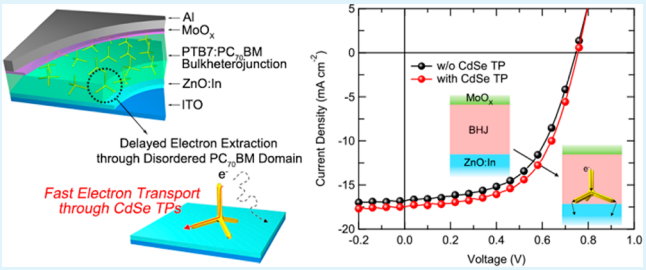

KEYWORDS: *nanostructured extraction layer, electron-selective interlayer, electron buffer layer, organic−inorganic hybrid solar cells, CdSe tetrapods, bulkheterojunction*

INTRODUCTION

In terms of device configuration in organic solar cells, an inverted structure, the electrons are collected by the bottom electrode−indium tin oxide (ITO), and holes are collected by the top electrode, has been steadily investigated.[1−4] Compared to conventional structure, inverted-type devices have potential for better long-term ambient stability by preventing the use of hygroscopic and acidic poly(3,4-ethylenedioxythiophene):poly-(styrenesulfonate) (PEDOT:PSS) as hole transport layer, which is detrimental to device lifetime.[5] In addition, by employing high work function metal for top electrode, the inverted device makes the low-cost roll-to-roll process possible as well as it has longer lifetime. One of the key factors in performance of inverted-type devices is the *n*-type buffer layer. This electron buffer layer should meet good optical transparency, electron transport and extraction characteristics with suitable energy band positions.

To collect photogenerated electrons efficiently from the active layer to cathode, the metal oxides thin films (e.g., SnO_2, TiO_2, and ZnO)[6−8] have been the most widely used as *n*-type buffer layers because of its properties of easy process, optical transparency, and good electrical performance. Furthermore, there have been efforts to make these metal oxides nanostructured, such as nanowires-, rods-, or wrinkles-shaped, to enhance the power conversion efficiency (PCE) of solar cells.[9−12] Because of their increased interfacial area and more continuous path for carrier transport,[10] short circuit current and overall performance of solar cells increased. However, to control the growth of these aligned metal oxides nanostructures, photolithography[13,14] or nanoimprint-soft lithography[9] was employed; both techniques are complicated fabrication methods using photoresist and exposure process. Therefore, it will be beneficial to find an easy-processable nanostructured interlayer regarding time and cost savings.

In the Research Article, we demonstrate a unique electron-selective interlayer comprising of In-doped ZnO (ZnO:In) and vertically aligned CdSe tetrapods (TPs) for polymer:fullerene bulkheterojunction (BHJ) solar cells. Using highly monodisperse CdSe TPs with tailored dimension for BHJ layer thickness, vertically electron transport channels were easily

Received: May 27, 2015
Accepted: August 3, 2015
Published: August 3, 2015

DOI: 10.1021/acsami.5b04624
ACS Appl. Mater. Interfaces 2015, 7, 18460−18466

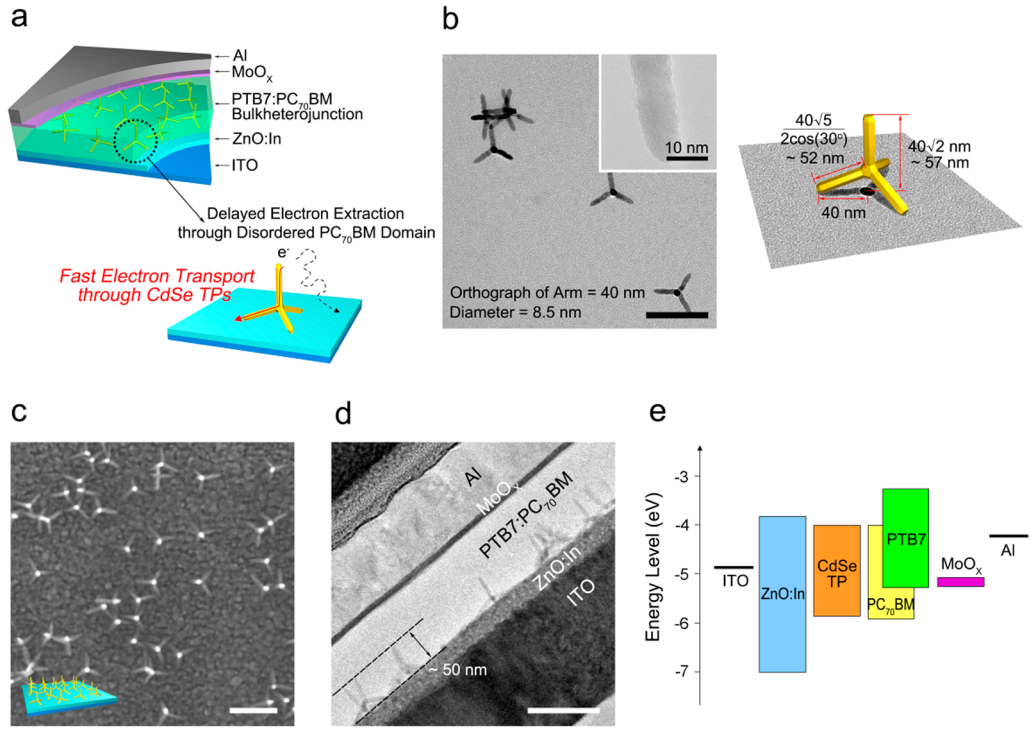

Figure 1. (a) Schematic illustration of a PTB7:$PC_{70}BM$ solar cell with the CdSe TP charge extraction nanostructure. The detailed role of CdSe TPs is illustrated below; CdSe TPs can extract photogenerated electrons in $PC_{70}BM$ domain by providing vertical transport pathway through their arms. (b) A transmission electron microscopy (TEM) image of CdSe TPs tailored for a PTB7:$PC_{70}BM$ BHJ layer. Detailed dimensions of vertically standing CdSe TPs are illustrated on the right. (c) A top scanning electron microscopy (SEM) image of the charge extraction nanostructure fabricated with 0.5 mg mL^{-1} of CdSe TP solution. (d) A cross-sectional TEM image of the PTB7:$PC_{70}BM$ solar cell with CdSe TPs. (e) An energy level diagram of PTB7:$PC_{70}BM$ solar cells with CdSe TPs. All scale bars are 100 nm.

assembled on the ZnO:In buffer layer by simple spin-coating process. In addition to good exciton dissociation properties of typical BHJ network with extensive interfaces, this CdSe TP nanostructures are able to offer direct and efficient pathways for photogenerated electrons from the active layer to ZnO:In buffer layer by penetrating the disordered BHJ domains, resulting in improved PCE to 7.55%.

RESULTS AND DISCUSSION

The organization of the hybrid solar cells with the charge extraction nanostructure is illustrated in Figure 1a. The vertically standing CdSe TPs were deposited on plane ZnO:In buffer layer/ITO cathode substrates. This nanostructure is assembled with poly[[4,8-bis[(2-ethylhexyl)oxy]benzo[1,2-b:4,5-b′]dithiophene-2,6-diyl][3-fluoro-2-[(2-ethylhexyl)carbonyl]thieno[3,4-*b*]thiophenediyl]] (PTB7):[6,6]-phenyl-C71-butyric acid methyl ester ($PC_{70}BM$) BHJ, and a molybdenum oxide (MoO_X) and an aluminum (Al) were evaporated as an anode. In this study, the colloidal CdSe TP nanocrystals were chosen because of their excellent electron mobility (bulk Hall electron mobility ~900 cm^2 V^{-1} s^{-1}),[15] appropriate energy levels (conduction band ~4 eV, Figure 1e), and structural uniqueness. These excellent electrical properties allow the electrons to be rapidly transferred from $PC_{70}BM$ (lowest unoccupied molecular orbital ~4 eV) to CdSe TPs and moved to the ZnO:In buffer layer. Therefore, the CdSe TPs are intended to amplify electron transport from $PC_{70}BM$ domains to the ITO cathode.

At the same time, the tetrapod morphology is the simplest architecture which can stably stand on a substrate owing to its low center of mass, so that vertically oriented inorganic channels can be easily produced by simple deposition of CdSe TPs on the substrate. In the present study, we synthesized morphologically uniform CdSe TPs (shape selectivity >90% and a deviation in arm length ~3 nm) with ~57 nm of theoretical height via the continuous precursor injection (CPI) method (Figure 1b).[16] The dimension of CdSe TPs was decided by the thickness of PTB7:$PC_{70}BM$ BHJ active layer varying from 70 to 100 nm. Taller CdSe TPs can possibly perforate the active layer and form an undesired contact with a MoO_X/Al layer. From a transmission electron microscopy (TEM) of CdSe TPs representing the orthographic projection image of CdSe TP arms, we could calculate the theoretical arm length (~52 nm) and 3-dimensional height (~57 nm) of CdSe TPs based on Pythagorean Theorem (Figure 1b).

Using the length-controlled CdSe TPs, the CdSe TPs were easily fabricated by spin-coating of solution and following thermal treatment. As shown in Figure 1c, CdSe TPs spun on the ZnO:In substrate formed a scattered morphology with vertically oriented arms (displaying as white dots). Besides, the heat treatment has a role in stratifying mechanical robustness of the CdSe TPs against following surface treatment and a formation of PTB7:$PC_{70}BM$ BHJ.[17] We confirmed that the morphology of CdSe TPs was preserved during ligand elimination (by repeating ethanol washing), surface passivation (with 1-hexylamine), and a formation of PTB7:$PC_{70}BM$ active layer (Figure S5). Note that high concentration (>3 mg mL^{-1}) of CdSe TP solution resulted in an entangled and directionless CdSe TP morphology, which is attributed to the capillary force between CdSe TPs during solvent drying (Figure S1). As shown in Figure 1d, the CdSe TP arms perpendicular to the ZnO:In substrate are included in the uniform PTB7:$PC_{70}BM$

DOI: 10.1021/acsami.5b04624
ACS Appl. Mater. Interfaces 2015, 7, 18460−18466

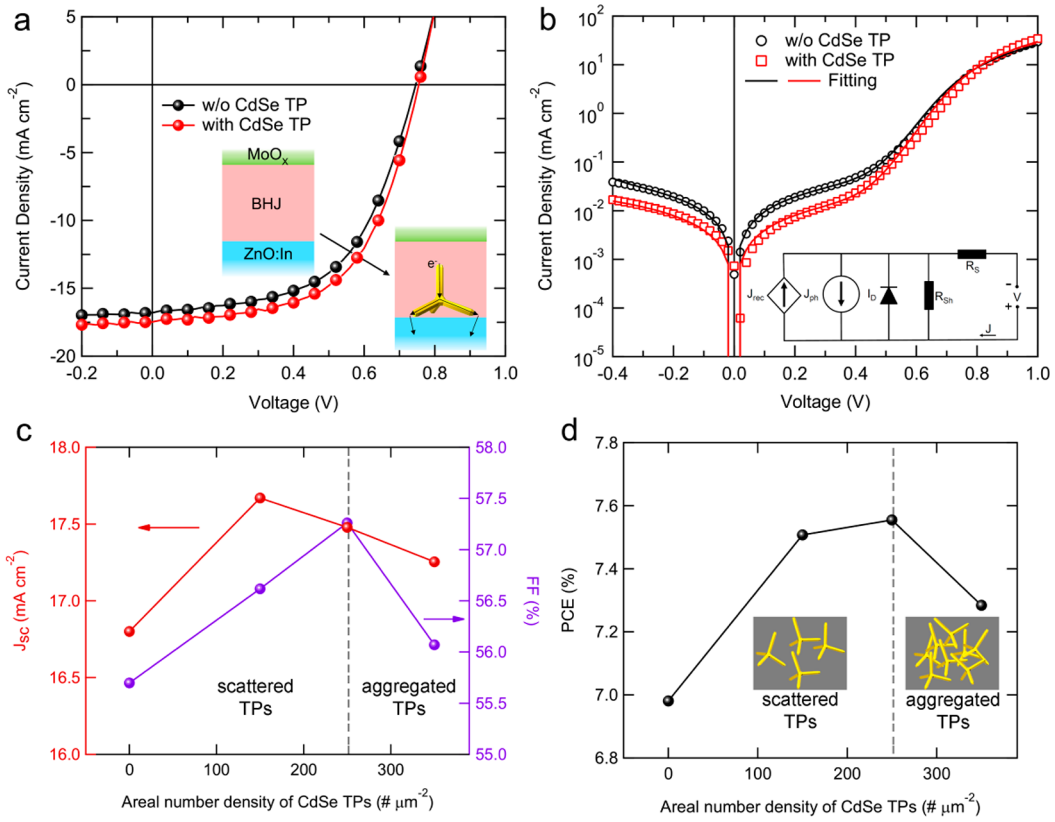

Figure 2. Current density (J)−voltage (V) characteristics of the PTB7:$PC_{70}BM$ solar cells without and with the 1 mg mL^{-1} of CdSe TPs, measured under the (a) AM1.5G 1 sun illumination and (b) dark condition. (c) Short circuit current density (J_{SC}), fill factor (FF), and (d) power conversion efficiency (PCE) as a function of the areal number density of CdSe TPs. The inset of panel b shows the equivalent circuit diagram for solar cells. Dark current fitting is done using this solar cell equivalent circuit model.

Table 1. Performance Parameters of Inverted PTB7:$PC_{70}BM$ Solar Cells without and with Different Concentration of Nanostructured CdSe TPs under AM 1.5G 1 Sun Illumination[a]

	J_{SC} (mA cm^{-2})	V_{OC} (V)	FF (%)	PCE (%)	R_S (Ω cm^2)	R_{SH} (Ω cm^2)
w/o CdSe TPs	16.82 ± 0.11 (16.80)	0.74 ± 0.01 (0.75)	55.22 ± 0.85 (55.70)	6.90 ± 0.10 (6.98)	8.30	532.34
with CdSe TPs (0.5 mg mL^{-1})	17.67 ± 0.08 (17.67)	0.75 ± 0.01 (0.75)	55.81 ± 0.71 (56.62)	7.39 ± 0.12 (7.51)	7.08	451.71
with CdSe TPs (1 mg mL^{-1})	17.46 ± 0.04 (17.48)	0.75 ± 0.01 (0.75)	56.30 ± 2.11 (57.26)	7.41 ± 0.27 (7.55)	6.70	539.14
with CdSe TPs (2 mg mL^{-1})	17.17 ± 0.10 (17.25)	0.75 ± 0.01 (0.75)	55.74 ± 0.83 (56.07)	7.17 ± 0.18 (7.28)	6.87	544.25

[a]The average and standard deviation values are for samples at least 4 devices on the same substrate. The values in brackets represent the photovoltaic parameters obtained for the best-performing cell.

active layer. Meanwhile, the overall height of CdSe TPs was estimated as ∼50 nm, slightly lower than the theoretical value. It is supposed to originate from the deviation in the arm length of CdSe TPs and the surface roughness of ZnO:In substrates (RMS roughness ∼1 nm).

Figure 2a shows the current density versus voltage (J−V) characteristics of solar cell devices without and with 1 mg mL^{-1} of CdSe TPs under the 1 sun illumination, and the results deduced from J−V curves are summarized in Table 1 together with the 0.5 and 2 mg mL^{-1} concentration of CdSe TPs. The device performance gradually improved when CdSe TPs were applied more as electron extraction interlayer as shown in Figure 2c and d, and the optimum device was achieved when 1 mg mL^{-1} of CdSe TP solution was used. Device containing 1 mg mL^{-1} of nanostructured CdSe TPs showed the improved short circuit current density (J_{SC}) and fill factor (FF) from 16.80 mA cm^{-2} and 55.70% to 17.48 mA cm^{-2} and 57.26%, respectively, while an open circuit voltage (V_{OC}) remains as same as the device without CdSe TP. Hence, the power conversion efficiency (PCE) increases from 6.98% to 7.55%. The CdSe TPs in this device absorbs some part of the UV−visible light as shown in Figure S6, however, this is negligible compared to the absorption of PTB7:$PC_{70}BM$, so that almost the whole absorption takes place in active layer. To quantify the numbers of CdSe TPs deposited on the ZnO:In film, we counted those of CdSe nanostructures within the small area of 0.12 μm^2 through the SEM images (Figure S3). The estimated number of CdSe TPs per unit surface area (μm^2) is 150, 250, and 350 when the concentration of CdSe TPs is 0.5, 1, and 2 mg mL^{-1}, respectively. As shown in Figure S4, this estimate is quite reasonable when we actually count the number of CdSe TPs with low magnification SEM image, because most tetrapods show well-distributed morphology in micrometer scale with proper fabrication condition (e.g., 0.5 mg mL^{-1}). As the further increase of concentration of CdSe TP solution to 2 mg mL^{-1}, device performance decreased. One possible reason is that the aggregated TP clusters with high concentration of CdSe TPs form voids, leading the reduction of the interfacial

DOI: 10.1021/acsami.5b04624
ACS Appl. Mater. Interfaces 2015, 7, 18460−18466

area between CdSe TPs and BHJ layer. Furthermore, the additional photogenerated charges from the high concentration of CdSe TPs may recombine before delivering the holes to polymer molecules due to its limited surface area with donor molecules. Therefore, the increased J_{SC} in the device with CdSe TPs is more attributed to the better charge transport of electrons, which are generated and dissociated in active layer, rather than the photogenerated electrons in CdSe TPs itself. The IPCE spectra (Figure S7) clearly prove that the improvement in the J_{SC} for the device with CdSe TP interlayer originates from the enhanced broad wavelength range of spectral response (300−800 nm). Note that all the devices with CdSe TPs, which concentration is up to 2 mg mL^{-1}, showed improved performance compared to the device without CdSe TP interlayer.

To investigate the effect of CdSe TPs (1 mg mL^{-1}) nanostructure into the electrical properties of the interface more systematically, the diode characteristics in the dark were studied. The dark $J-V$ curves of the solar cells without and with CdSe TPs are shown in Figure 2b, and equivalent circuit model is shown in inset of Figure 2b. With no illumination ($J_{ph} = J_{rec} = 0$) and in the regime where diode characteristics are dominant, that is, $\exp[q(V-JR_S)/nkT] \gg 1$, the current density−voltage equation can be expressed as shown in eq 1[18]

$$\ln\left(J - \frac{V - JR_S}{R_{SH}}\right) = \ln J_0 + \frac{q}{nkT}(V - JR_S) \quad (1)$$

where J_0 and n represent the reverse saturation current density and diode ideality factor, respectively, q is the elementary charge, k is the Boltzmann constant, T is the absolute temperature, J_{ph} is the photogenerated current density, J_{rec} is the additional loss term taken place within the active layer of the device,[19] R_S is the series resistance, and R_{SH} is the shunt resistance. The parameters of J_0 and n can be evaluated from the y-intercept and the slope of the line, respectively. The solid lines in Figure 2b show the fitted results, while circles and triangles represent the measured values of dark current density, and the set of parameters extracted from these are summarized in Table 2. With vertically aligned nanostructure of CdSe TPs

Table 2. Fitted Parameters Calculated from the Dark Curve of PTB7:PC$_{70}$BM Solar Cells without and with Nanostructured CdSe TPs

	J_0 (nA cm^{-2})	n	R_S (Ω cm^2)	R_{SH} (kΩ cm^2)
w/o CdSe TP	1.68	1.82	8.55	10.54
with CdSe TP (1 mg mL^{-1})	1.03	1.79	6.83	25.28

in solar cell device, the reverse saturation current density and series resistance decreased, and the shunt resistance increased, as well as the diode ideality factor was closer to 1. The lower reverse saturation current density in the device with CdSe TPs means that the diffusion of minority carriers, which are holes in our case, is smaller. At the same time, current is higher at the positive voltage around 1 V, and therefore CdSe TPs can work as electron-selective layer both transporting electrons and blocking holes. The two times higher value of shunt resistance for the device with CdSe TPs also implies that the leakage current is effectively suppressed by the CdSe TPs layer.[20] The diode ideality factor n is known as reflecting the properties of the internal BHJ morphology,[21] recombination loss or disorder in the electronic states.[22,23] The n value of the device having CdSe TPs is closer to 1, and it can be interpreted as decrease of the interfacial recombination with the introduced CdSe TPs. The characteristics of recombination and charge collection for the devices without and with CdSe TPs will be discussed below. To sum up these $J-V$ curve under the illumination and dark diode characteristics, we conclude that CdSe TPs with ZnO:In layer work as nanostructured electron-selective layer, which can extract electrons well from the disordered PC$_{70}$BM domain to the cathode through their vertically aligned inorganic domains, resulting in improved J_{SC} and FF.

To explore the effects of CdSe TPs on carrier recombination and collection characteristics, we determined the light intensity dependence of J_{SC} and V_{OC}, and collection voltages (V_C) of the solar cell devices without and with CdSe TPs. First of all, Figure 3a shows the log−log plot of incident light dependence of J_{SC} of the devices, and the J_{SC} values change linearly along the light intensity for the both, yielding the power law of 0.894 for the device without CdSe TPs and 0.914 for the one with CdSe TPs. When the exponent value closes to 1, then extraction of charge carriers is faster than recombination, so that recombination mechanism is dominated by monomolecular recombination, while it closes to 0.5 if bimolecular recombination is dominant due to comparable processes between charge extraction and recombination.[24,25] Therefore, the higher value for the device with CdSe TPs means that bimolecular recombination losses are more suppressed than the device without CdSe TPs. Second, the values of V_{OC} as a function of light intensity were measured to determine the additional recombination mechanism of trap-assisted recombination, which is a Shockley-Read-Hall (SRH) recombination, as shown in Figure 3b. A slope of thermal voltage (kT/q) features the strength of the recombination: the higher slope correlates with the more charge recombination losses.[26,27] The linear slope of V_{OC}−log(P_{light}) is 1.36 kT/q for a solar cell without CdSe TPs, whereas 1.29 kT/q for a cell with CdSe TPs, implying that the device with CdSe TPs has less trap-assisted recombination loss, and fewer trap states than the one without CdSe TPs. To obtain further investigation into the collection properties of solar cells depending on the existence of CdSe TPs, we last analyzed the collection voltage (V_C). As shown in Figure 3c and d, collection voltages (V_C) can be defined by a crossing point of all linear fits for the J-V curves, which were measured at various light intensity (5−100 mW cm^{-2}), at short circuit condition. We can calculate the collection efficiency at short circuit condition (η_{C0}) and effective $\mu\tau$ product ($\mu\tau_{eff}$) from the V_C. Recently, Voz et al.[19] employed the V_C to calculate carrier collection efficiency (η_C) in polymer solar cells under the three assumptions, which are constant electric field, drift-driven collection, and monomolecular recombination. For an equivalent circuit of solar cells, as shown in the inset of Figure 2b, the J_{rec} term was introduced, since a significant recombination occurs within the active layer of the solar cells consisting of disordered materials, such as amorphous silicon or organic materials. Under the above assumptions, the collection efficiency of photogenerated charge carriers at short circuit condition (η_{C0}), short circuit resistance (R_{SC}, reciprocal slopes of the $J-V$ curve at $V = 0$, that is, $V_C = R_{SC}\,J_{SC}$), which reflects the recombination term (J_{rec}) under the various light intensities, and V_C can be expressed as

$$\eta_{C0} = 1 - \frac{L/2}{l_{C0}} \quad (2)$$

DOI: 10.1021/acsami.5b04624
ACS Appl. Mater. Interfaces 2015, 7, 18460−18466

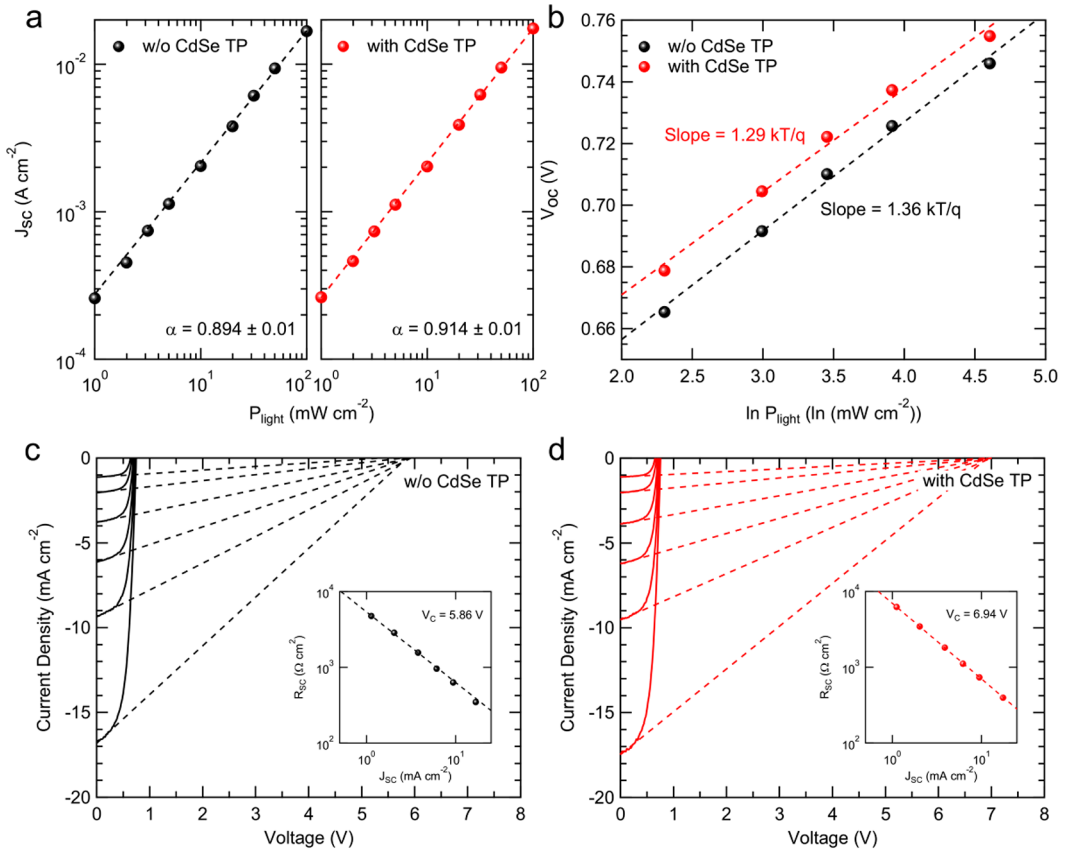

Figure 3. (a) Light intensity dependence of short circuit current density (J_{SC}) for cells without and with CdSe TPs. Dotted lines show fitting curves using a power law. (b) Open circuit voltage (V_{OC}) of cells without and with CdSe TPs as a function of light intensity, together with linear fits. (c and d) $J-V$ characteristics of cells without and with CdSe TPs measured at various incident light intensity (5−100 mW cm^{-2}). Collection voltages (V_C) are defined by the intersection of all linear fits at short circuit condition. The insets of panels c and d show R_{SC} extracted around $V = 0$, and calculated V_C from the relation of $V_C = R_{SC}J_{SC}$.

$$R_{SC} = \left(\frac{l_{C0}}{L/2} - 1\right)\frac{V_{bi}}{J_{SC}} \tag{3}$$

$$V_C = \left(\frac{l_{C0}}{L/2} - 1\right)V_{bi} \tag{4}$$

with

$$l_{C0} = \mu\tau_{eff}\frac{V_{bi}}{L} \tag{5}$$

where l_{C0} is the collection length at short circuit condition, L is a thickness of the active layer, $\mu\tau_{eff}$ is the effective $\mu\tau$ product, that is, $\mu\tau_{eff} = \mu_n\tau_n + \mu_p\tau_p$, and V_{bi} is the built-in potential, which refers to the voltage at which J_{ph} is zero, where J_{ph} is determined as subtracting measured current density in the dark from the measured current density under illumination.[26] The collection length denotes the maximum distance of dissociated electrons and holes driven by the electric field before recombination. The detailed derivations of formulas are given in the reference quoted above. The values of V_C are 5.86 and 6.94 V for the device without CdSe TPs and with CdSe TPs, respectively, as shown in Figure 3c and d. According to the eq 2 and 4 with an active layer thickness of 90 nm, the η_{C0} increases from 85.4% to 88.3% by inserting nanostructured CdSe TPs between ZnO:In and active layer. The corresponding $\mu\tau_{eff}$ product using an eq 5 is 2.8×10^{-10} cm^2 V^{-1} for the cell without CdSe TPs, whereas 3.8×10^{-10} cm^2 V^{-1} for the cell with CdSe TPs. These calculated parameters of η_{C0} and $\mu\tau_{eff}$ indicate that CdSe TPs provide the better charge transport and extraction characteristics through their vertically aligned arms, which straight connect the active layer to buffer layer, and in the end to the electrode.

CONCLUSIONS

In conclusion, we studied the roles of CdSe TPs as an electron-selective interlayer on the performance of inverted organic solar cells. By providing the direct inorganic path from the disordered BHJ domain to electron buffer layer, CdSe TPs layer can effectively extract photogenerated charge carriers, leading to the improvement of both J_{SC} and FF of the solar cell devices. It was demonstrated that CdSe TPs reduce the interfacial traps between the BHJ layer and buffer layer, reduce the recombination losses, improve the hole-blocking properties as well as electron-transporting, and therefore improve charge collection. Consequently, the PCE of PTB7:$PC_{70}BM$ based solar cell with nanostructured CdSe TPs increases to 7.55%. These results indicate that this method introduced herein, which uses the length-controlled inorganic nanocrystals as an interlayer, can be generally applicable to various organic solar cells.

EXPERIMENTAL METHODS

Materials. Cadmium oxide powder (CdO, 99.95%) was obtained from Alfa Aesar. Selenium powder (99.99%), oleic acid (OA, 90%), *n*-trioctylphosphine (TOP, 90%), 1-octadecene (1-ODE, 90%),

DOI: 10.1021/acsami.5b04624
ACS Appl. Mater. Interfaces 2015, 7, 18460−18466

hexadecyltrimethylammonium bromide (HTAB, 99+%), chlorobenzene (99.8%), zinc acetate dihydrate ($Zn(ac)_2{\cdot}2H_2O$, ≥ 98%), indium(III) nitrate hydrate ($In(NO_3)_3{\cdot}xH_2O$, 99.99%), ethanolamine (≥99.0%), and 1-hexylamine (99%) were purchased from Sigma-Aldrich. PTB7, $PC_{70}BM$, and 1,8-diiodooctane were purchased from 1-Material, American Dye Source Inc., and Tokyo Chemical Industry Co., respectively. All materials were used as received.

Synthesis of CdSe TP and Surface Modification. Synthetic process by Lim et al.[16] was partially modified to prepare arm length-controlled CdSe TPs. As arm growth precursors, cadmium oleate ($Cd(OA)_2$) solution (reacting 10 mmol of CdO with 9 mL of OA in 5 mL of ODE and 1 mL of TOP at 280 °C) containing 0.14 mmol of HTAB and SeTOP solution (reacting 12 mmol Se with 6 mL TOP at 150 °C) were mixed under inert atmosphere for 5 min. Then, 28 mL of the arm growth precursors was continuously injected into the seed solution (0.3 μmol of CdSe seeds (diameter ∼5 nm) dissolved in 26.25 mL of ODE, 1.5 mL of TOP, 2.25 mL of OA, and 0.21 mmol of HTAB) at 260 °C. Injection rate was fixed to 30 mL/h. After the precursor injection was finished, the crude solution was immediately cooled down to ambient temperature and purified three times using acetone (for precipitation) and hexane (for redispersion). The final product was dispersed in hexane for surface modification.

Oleate ligands of CdSe TPs were replaced with oleylamine via two-phase ligand exchange procedure.[17] Briefly, oleate-capped CdSe TPs dispersed in nonpolar organic phase (e.g., hexane) and polar DMF phase containing HBF_4 were put in a round-bottom flask and vigorously stirred to transfer the CdSe TPs to the DMF phase, which indicates the elimination of oleate ligands. Next, the bare CdSe TPs dispersed in the DMF phase were precipitated using acetone and redispersed in a mixture of chloroform and oleylamine (for example, 4 mL of chloroform and 1 mL of oleylamine). Then, the oleylamine-capped CdSe TPs were precipitated using acetone to remove excess oleylamine. Finally, chloroform was added to the precipitates to disperse CdSe TPs. Small amount of oleylamine was helpful to sustain colloidal stability of CdSe TPs over several weeks.

Preparation of ZnO:In/CdSe TP Charge Extraction Nanostructure. In-doped ZnO thin films (ZnO:In) have been prepared by spin-coating of sol–gel precursor. $Zn(ac)_2{\cdot}2H_2O$ and $In(NO_3)_3{\cdot}xH_2O$ (5 at. % of the precursor) were dissolved in a mixture of ethanol and ethanolamine (ethanol/ethanolamine = 10:0.15 (v/v)) and stirred for 2 h at room temperature to yield a homogeneous and clear solution. Then, as-prepared precursor solution was spin-coated on a ultraviolet-ozone treated ITO-coated glass at 3500 rpm for 40 s and sequentially annealed in atmosphere from 120 to 450 °C for 2 h, resulting in 30 nm-thick ZnO:In thin films.

To assembly CdSe TPs, the ZnO:In substrates were transferred to a glovebox filled with Ar. One mg mL^{-1} of CdSe TP solution was spun at 2000 rpm for 30 s on top of the ZnO:In substrate, followed by annealing at 150 °C for 20 min. Following, the film was washed twice using ethanol at room temperature and annealed at 120 °C for 10 min to remove residual solvent and fix CdSe TPs on the ZnO:In substrate. Then, the CdSe TPs was modified with 1-hexylamine (acetone/1-hexylamine = 8:2 (v/v)) by spin-coating at 2000 rpm and dried at 100 °C for 10 min. Note that the series of thermal annealing and use of solvents showed no significant differences in electrical property of ZnO:In thin films.

Fabrication and Characterization of Solar Cells. Twenty-five milligrams per milliliter of PTB7:$PC_{70}BM$ blend with a weight ratio of 2:3 dissolved in mixed solvent (chlorobenzene/1,8-diiodooctane (97:3 (v/v)) was spin-coated onto the CdSe TP electron extraction interlayer at 1000 rpm for 60 s; the thickness of active layer is about 90 nm. Subsequently, 10 nm of MoO_X and 100 nm of Al layers were thermally evaporated under a 10^{-6} Torr vacuum. The active areas of solar cells, defined by the overlap between ITO and Al electrodes, were 1.96 mm^2. The current density–voltage (J–V) characteristics of the solar cell devices were measured with a source measurement unit (Keithley SMU237). The performances of the devices were characterized under AM1.5G solar spectrum at 1 sun (100 mW cm^{-2}) illumination, simulated by Newport 91160A. Light power was controlled using neutral density filters from 5 mW cm^{-2} to 100 mW cm^{-2}. The incident photon-to-current conversion efficiency (IPCE) spectra of devices were acquired using an Oriel IQE 200 model, which composed of xenon lamp, lock-in amplifier, and monochromator with slit wheels, order sorting filters, and gratings.

Characterization of Charge Extraction Nanostructure. The absorption spectra of charge extraction nanostructure were measured on a PerkinElmer Lambda 35 UV–visible spectrophotometer. Surface morphology of ZnO:In/CdSe TP film was obtained using scanning electron microscopy (JEOL JSM-6701F). Cross-sectional image of solar cells were taken using focused-ion beam equipment (FEI Nova 600 Nanolab) for sample preparation and transmission electron microscopy (JEOL JEM-2100F).

■ ASSOCIATED CONTENT

Supporting Information

The Supporting Information is available free of charge on the ACS Publications website at DOI: 10.1021/acsami.5b04624.

SEM image of colloidal CdSe TPs, a cross-sectional TEM image of PTB7:$PC_{70}BM$ solar cells and its elemental mapping, the areal number density of CdSe TPs with different concentration, SEM images of CdSe TP film showing its robustness, absorption spectra of CdSe TPs and PTB7:$PC_{70}BM$, and IPCE spectra of solar cells without and with CdSe TPs (PDF)

■ AUTHOR INFORMATION

Corresponding Authors

*E-mail: khchar@plaza.snu.ac.kr.

*E-mail: chlee7@snu.ac.kr.

Author Contributions

‖J.S. and J.L. contributed equally.

Notes

The authors declare no competing financial interest.

■ ACKNOWLEDGMENTS

This work was supported by the Human Resources Development program (No. 20124010203170) of the Korea Institute of Energy Technology Evaluation and Planning (KETEP) grant funded by the Korea government Ministry of Trade, Industry, and Energy. This work was also financially supported by the National Research Foundation of Korea (NRF) grant funded by the Korea government Ministry of Science, ICT & Future Planning (MSIP): the National Creative Research Initiative Center for Intelligent Hybrids (No. 2010-0018290), the WCU Program of C2E2 (R31-10013), the Technology Development Program to Solve Climate Changes (NRF-2009-0093304, NRF-2014R1A2A1A11054246, and NRF-2009-0093319), the Global Frontier R&D Program on Center for Multiscale Energy System (2011-0031567), and the Brain Korea 21 Plus Project in 2015.

■ REFERENCES

(1) He, Z.; Zhong, C.; Su, S.; Xu, M.; Wu, H.; Cao, Y. Enhanced Power-Conversion Efficiency in Polymer Solar Cells Using an Inverted Device Structure. *Nat. Photonics* **2012**, *6*, 591–595.

(2) You, J.; Dou, L.; Yoshimura, K.; Kato, T.; Ohya, K.; Moriarty, T.; Emery, K.; Chen, C.-C.; Gao, J.; Li, G.; Yang, Y. A Polymer Tandem Solar Cell with 10.6% Power Conversion Efficiency. *Nat. Commun.* **2013**, *4*, 1446.

(3) Small, C. E.; Chen, S.; Subbiah, J.; Amb, C. M.; Tsang, S.-W.; Lai, T.-H.; Reynolds, J. R.; So, F. High-Efficiency Inverted Dithienogermole-Thienopyrrolodione-Based Polymer Solar Cells. *Nat. Photonics* **2011**, *6*, 115–120.

DOI: 10.1021/acsami.5b04624
ACS Appl. Mater. Interfaces 2015, 7, 18460–18466

(4) Liao, S.-H.; Jhuo, H.-J.; Yeh, P.-N.; Cheng, Y.-S.; Li, Y.-L.; Lee, Y.-H.; Sharma, S.; Chen, S.-A. Single Junction Inverted Polymer Solar Cell Reaching Power Conversion Efficiency 10.31% by Employing Dual-Doped Zinc Oxide Nano-Film as Cathode Interlayer. *Sci. Rep.* **2014**, *4*, 6813.
(5) Voroshazi, E.; Verreet, B.; Buri, A.; Müller, R.; Di Nuzzo, D.; Heremans, P. Influence of Cathode Oxidation via the Hole Extraction Layer in Polymer:Fullerene Solar Cells. *Org. Electron.* **2011**, *12*, 736−744.
(6) Kim, Y. S.; Yu, B.-K.; Kim, D.-Y.; Kim, W. B. A Hybridized Electron-Selective Layer Using Sb-Doped SnO_2 Nanowires for Efficient Inverted Polymer Solar Cells. *Sol. Energy Mater. Sol. Cells* **2011**, *95*, 2874−2879.
(7) Kim, J. Y.; Kim, S. H.; Lee, H.-H.; Lee, K.; Ma, W.; Gong, X.; Heeger, A. J. New Architecture for High-Efficiency Polymer Photovoltaic Cells Using Solution-Based Titanium Oxide as an Optical Spacer. *Adv. Mater.* **2006**, *18*, 572−576.
(8) Hau, S. K.; Yip, H.-L.; Baek, N. S.; Zou, J.; O'Malley, K.; Jen, A. K.-Y. Air-Stable Inverted Flexible Polymer Solar Cells Using Zinc Oxide Nanoparticles as an Electron Selective Layer. *Appl. Phys. Lett.* **2008**, *92*, 253301.
(9) Kim, S.; Kim, C.-H.; Lee, S. K.; Jeong, J.-H.; Lee, J.; Jin, S.-H.; Shin, W. S.; Song, C. E.; Choi, J.-H.; Jeong, J.-R. Highly Efficient Uniform ZnO Nanostructures for an Electron Transport Layer of Inverted Organic Solar Cells. *Chem. Commun.* **2013**, *49*, 6033−6035.
(10) Liu, J.; Wang, S.; Bian, Z.; Shan, M.; Huang, C. Organic/Inorganic Hybrid Solar Cells with Vertically Oriented ZnO Nanowires. *Appl. Phys. Lett.* **2009**, *94*, 173107.
(11) Lee, Y.-J.; Lloyd, M. T.; Olson, D. C.; Grubbs, R. K.; Lu, P.; Davis, R. J.; Voigt, J. A.; Hsu, J. W. P. Optimization of ZnO Nanorod Array Morphology for Hybrid Photovoltaic Devices. *J. Phys. Chem. C* **2009**, *113*, 15778−15782.
(12) Seo, H. O.; Park, S.-Y.; Shim, W. H.; Kim, K.-D.; Lee, K. H.; Jo, M. Y.; Kim, J. H.; Lee, E.; Kim, D.-W.; Kim, Y. D.; Lim, D. C. Ultrathin TiO_2 Films on ZnO Electron-Collecting Layers of Inverted Organic Solar Cell. *J. Phys. Chem. C* **2011**, *115*, 21517−21520.
(13) Tak, Y.; Yong, K. Controlled Growth of Well-Aligned ZnO Nanorod Array Using a Novel Solution Method. *J. Phys. Chem. B* **2005**, *109*, 19263−19269.
(14) Ahsanulhaq, Q.; Kim, J. H.; Hahn, Y.-B. Etch-Free Selective Area Growth of Well-Aligned ZnO Nanorod Arrays by Economical Polymer Mask for Large-Area Solar Cell Applications. *Sol. Energy Mater. Sol. Cells* **2012**, *98*, 476−481.
(15) Adachi, S. *Properties of Semiconductor Alloys: Group-IV, III-V and II-VI Semiconductors*; Wiley: Hoboken, NJ, 2009; p 366.
(16) Lim, J.; Bae, W. K.; Park, K. U.; zur Borg, L.; Zentel, R.; Lee, S.; Char, K. Controlled Synthesis of CdSe Tetrapods with High Morphological Uniformity by the Persistent Kinetic Growth and the Halide-Mediated Phase Transformation. *Chem. Mater.* **2013**, *25*, 1443−1449.
(17) Lim, J.; Lee, D.; Park, M.; Song, J.; Lee, S.; Kang, M. S.; Lee, C.; Char, K. Modular Fabrication of Hybrid Bulk Heterojunction Solar Cells Based on Breakwater-like CdSe Tetrapod Nanocrystal Network Infused with P3HT. *J. Phys. Chem. C* **2014**, *118*, 3942−3952.
(18) Lee, J. H.; Cho, S.; Roy, A.; Jung, H.-T.; Heeger, A. J. Enhanced Diode Characteristics of Organic Solar Cells Using Titanium Suboxide Electron Transport Layer. *Appl. Phys. Lett.* **2010**, *96*, 163303.
(19) Voz, C.; Puigdollers, J.; Asensi, J. M.; Galindo, S.; Cheylan, S.; Pacios, R.; Ortega, P.; Alcubilla, R. Analysis of the Dynamic Short-Circuit Resistance in Organic Bulk-Heterojunction Solar Cells: Relation to the Charge Carrier Collection Efficiency. *Org. Electron.* **2013**, *14*, 1643−1648.
(20) Steim, R.; Choulis, S. A.; Schilinsky, P.; Brabec, C. J. Interface Modification for Highly Efficient Organic Photovoltaics. *Appl. Phys. Lett.* **2008**, *92*, 093303.
(21) Waldauf, C.; Scharber, M. C.; Schilinsky, P.; Hauch, J. A.; Brabec, C. J. Physics of Organic Bulk Heterojunction Devices for Photovoltaic Applications. *J. Appl. Phys.* **2006**, *99*, 104503.
(22) Garcia-Belmonte, G. Carrier Recombination Flux in Bulk Heterojunction Polymer:Fullerene Solar Cells: Effect of Energy Disorder on Ideality Factor. *Solid-State Electron.* **2013**, *79*, 201−205.
(23) van Berkel, C.; Powell, M. J.; Franklin, A. R.; French, I. D. Quality Factor in *a*-Si:H *nip* and *pin* Diodes. *J. Appl. Phys.* **1993**, *73*, 5264−5268.
(24) Schilinsky, P.; Waldauf, C.; Brabec, C. J. Recombination and Loss Analysis in Polythiophene Based Bulk Heterojunction Photodetectors. *Appl. Phys. Lett.* **2002**, *81*, 3885−3887.
(25) Riedel, I.; Parisi, J.; Dyakonov, V.; Lutsen, L.; Vanderzande, D.; Hummelen, J. C. Effect of Temperature and Illumination on the Electrical Characteristics of Polymer−Fullerene Bulk-Heterojunction Solar Cells. *Adv. Funct. Mater.* **2004**, *14*, 38−44.
(26) Cowan, S. R.; Roy, A.; Heeger, A. J. Recombination in Polymer-Fullerene Bulk Heterojunction Solar Cells. *Phys. Rev. B: Condens. Matter Mater. Phys.* **2010**, *82*, 245207.
(27) Kyaw, A. K. K.; Wang, D. H.; Wynands, D.; Zhang, J.; Nguyen, T.-Q.; Bazan, G. C.; Heeger, A. J. Improved Light Harvesting and Improved Efficiency by Insertion of an Optical Spacer (ZnO) in Solution-Processed Small-Molecule Solar Cells. *Nano Lett.* **2013**, *13*, 3796−3801.

DOI: 10.1021/acsami.5b04624
ACS Appl. Mater. Interfaces 2015, 7, 18460−18466